

# Sensor Self-Localization for Antenna Arrays Subject to Bending and Vibrations

**AGNÈS SANTORI**

ONERA  
France

**JEAN BARRÈRE**

**GILLES CHABRIEL**  
**CLAUDE JAUFFRET**

Université du Sud Toulon-Var  
CNRS, IM2NP (UMR 6242)

**DOMINIQUE MEDYNSKI**

ONERA  
France

**A method is presented for dealing with the array self-calibration problem with persistent and noncooperating narrowband sources such as TV, GSM, and radio emissions. We consider large and flexible antennas whose sensors are subject to important static distortions and dynamical vibrations. Such antennas can be found, for example, when a high-resolution array is inserted along the wings of an aircraft. We propose a self-calibration technique that solves phase ambiguities arising from the large static bending and estimates the current array shape. This two-step method can be used with a single carrier frequency or with multiband sensors. The performance of the method is evaluated with simulated data and is compared to the Cramér-Rao lower bound (CRLB).**

Manuscript received July 17, 2007; revised June 13, 2008 and January 30, 2009; released for publication February 19, 2009.

IEEE Log No. T-AES/46/2/936823.

Refereeing of this contribution was handled by A. Lanterman.

Authors' addresses: A. Santori and D. Medynski, Dept. of Radar and Electromagnetism, ONERA, BA 701, 13661 Salon Air, France; J. Barrère, G. Chabriel, and C. Jauffret, Université du Sud Toulon-Var, GESSY, Avenue de l'université, BP 20132, La Garde CEDEX, 83957, France, E-mail: (chabriel@univ-tln.fr).

0018-9251/10/\$26.00 © 2010 IEEE

## I. INTRODUCTION

Several authors have studied the influence of array shape calibration errors on the direction of arrival (DOA) estimation problem (see, e.g., [1, 2]). They showed that direction finding with sensor arrays requires the knowledge of sensor locations. High angular accuracy demands large sensor arrays. In practice, such antennas are integrated into structures exposed to significant unknown distortions and vibrations.

The sensor array calibration using multiple beacon signals, disjoint in time or in frequency, has been studied in numerous papers (see, e.g., [3–6]). When such sources are not available, as in our case, a self-calibration must be achieved using signals of opportunity, i.e., with unknown DOA, often observed at the same frequency cell and at the same time.

For a static (no vibrating) case and for small calibration errors, the observability of the sensor localization problem was initially studied by Rockah and Schultheiss [4]; they showed that in a two-dimensional (2D) problem, three broadband sources are necessary for calibrating the array, provided that the exact location of one sensor and the direction of another one are known. The self-calibration problem with a single but moving source has been treated in [7].

When nondisjoint sources are considered, Weiss and Friedlander presented a sensor self-localization method based on the maximum-likelihood technique for narrowband sources and for omnidirectional sensors [8]. They used a numerical routine that iterates alternatively between DOAs of sources and sensor locations. The initialization step is performed by the MUSIC algorithm, which is computed with at-rest sensors' locations. In [9], the same authors developed a direct method called the constant modulus algorithm (CMA), directly exploiting omnidirectional sensors to separately identify the elements of the complex array response matrix. In [10], Flanagan and Bell suggested a method for dealing with higher static distortion magnitudes, inspired by [8].

All the cited approaches assume static and small calibration errors, i.e., smaller than half the wavelength of the recorded sources. When higher distortions are considered, phase ambiguity problems yield false (or ghost) locations. In [11], Marcos introduced a method using the propagation operator. Using a partially calibrated array, it calibrates highly distorted arrays composed of close sensors.

This paper, which is an extended version of [13], presents a method for dealing with the array shape self-calibration problem, based on persistent and noncooperating sources such as TV, GSM, or radio emissions. The antennas considered here are inserted along a large and flexible aircraft wing; as

a consequence, sensors are simultaneously subject to a large static distortion and dynamical vibrations. In addition, the antennas are sparse.

The size of the wing on which the antenna is mounted can exceed 10 m, and the maximum deformation can reach up to 1 m at the wing tip, i.e., greater than the typical wavelengths ( $\lambda$ ). Conversely, we assume that deformations near the fuselage are negligible. Generally, only the very low frequency vibrating modes ( $< 10$  Hz) are significant. Their magnitudes can reach up to roughly 10% of the maximum static deformation in steady flight, i.e., lower than the typical wavelengths.

The paper is organized as follows. Section II states the problem and presents the data model used to describe the recordings provided by a large distorted and vibrating array. In Section III, under a noise-free assumption, a new formulation of CMA is presented to estimate the array response matrix. Then, we study the phase ambiguity problem and propose a solution. A new necessary and sufficient condition for position observability is given in Appendix B. Section IV deals with noise. Once more inspired by CMA, we propose a two-step method that first estimates the static array shape and then estimates the current array shape. The two-step method briefly introduced in [13] is elaborated here, and extended to dual-band sensor arrays in Section V. The last section is devoted to numerical simulations and comparisons to Cramér-Rao lower bounds (CRLB).

## II. PROBLEM FORMULATION AND DATA MODEL

We consider  $N$  narrowband sources with the same carrier frequency ( $N$  is assumed known) and an array composed of  $M$  omnidirectional and identical sensors ( $M > N$ ). All are assumed to be in the same geometrical plane. The position of the first two sensors are known and are used to define the origin and the  $x$ -axis of the coordinate system; see Fig. 1. The distance between them is lower than or equal to half the wavelength  $\lambda$  of the carrier frequency. In this coordinate system, the current position vector of the  $i$ th sensor is defined by

$$\mathbf{p}_i(t) = [x_i(t), z_i(t)]^T. \quad (1)$$

Nominal sensor locations (for example, corresponding to the antenna at rest) are known. The intersensor distance, except the distance between the first two sensors, can be greater than  $\lambda/2$ . In the same way, the distance between the current location and at-rest location of a sensor can be greater than  $\lambda/2$ ; this justifies the expression “large deformations.”

With the axis system described in Fig. 1, the DOA of the  $j$ th source is given by the unit vector

$$\mathbf{n}_j = [\sin(\theta_j), \cos(\theta_j)]^T. \quad (2)$$

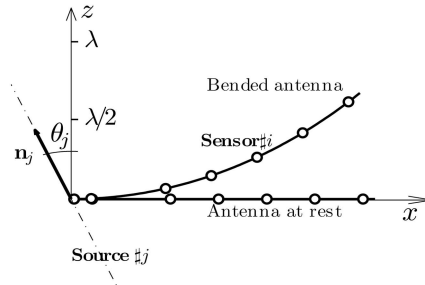


Fig. 1. Antenna shape and sensor locations.

All sources are land based and in the same half-plane:  $-\pi/2 < \theta_j < \pi/2$  for all  $j \in \{1, \dots, N\}$ . The DOA of each source is the same for all sensors (far-field assumption). We assume there is no multipath since the signals originate from the ground.

We let  $\mathbf{s}(t) = [s_1(t), \dots, s_N(t)]^T$  be the vector of the  $N$  baseband sources. The different sources are assumed to be ergodic, stationary, and zero-mean random processes. The signal at the output of the sensors can be described by the  $M$ -dimensional vector  $\mathbf{y}(t) = [y_1(t), \dots, y_M(t)]^T$  as

$$\mathbf{y}(t) = \mathbf{A}(t)\mathbf{s}(t) + \boldsymbol{\eta}(t) \quad (3)$$

where  $\boldsymbol{\eta}(t)$  is the noise vector. By assumption, each component  $\eta_i(t)$  ( $i = 1 \dots M$ ) of the noise is an ergodic, stationary, and zero-mean random process. Moreover, it is spatially and temporally white with the power  $\eta^2$  on each sensor. The matrix  $\mathbf{A}(t)$  stands for the  $(M \times N)$  array response matrix. The columns of  $\mathbf{A}(t)$  are the steering vectors of each source. The DOA of each source is assumed distinct, so  $\mathbf{A}(t)$  is full column rank. Since the sensors are omnidirectional and identical, the modulus of each component of the matrix  $\mathbf{A}(t)$  is constant. It is taken equal to one without loss of generality.

Under these assumptions, an entry  $a_{ij}(t)$  of  $\mathbf{A}(t)$  can be expressed as

$$a_{ij}(t) = \exp \left\{ j \frac{2\pi}{\lambda} \mathbf{p}_i^T(t) \mathbf{n}_j \right\}. \quad (4)$$

Since the first sensor is the origin of the coordinate system,

$$a_{1j}(t) = 1, \quad \forall j.$$

We propose estimating the array response matrix  $\mathbf{A}(t)$  to extract the sensor locations  $\mathbf{p}_i(t)$  for all  $i \in \{3, \dots, M\}$ .

## III. SELF-CALIBRATION IN A NOISE-FREE CASE: A DIRECT METHOD FOR LARGE DEFORMATIONS

### A. Array Response Matrix Estimation

The following derivations are inspired by the CMA proposed by van der Veen and Paulraj [12] and adapted to the self-calibration problem by Weiss and Friedlander [9].

From (3), the sampled data model in the noise-free case becomes  $\mathbf{y}(t_k) = \mathbf{A}(t_k)\mathbf{s}(t_k)$ , ( $k = 1, \dots, N_s$ ).

*Local Stationarity Assumption:* We assume that the sampling frequency is chosen sufficiently high and the sample number  $N_s$  sufficiently small such that the matrix  $\mathbf{A}(t_k)$  is locally time independent; hence, in this section,  $\mathbf{A}$  stands for  $\mathbf{A}(t_k)$ , at times  $t_k$  ( $k = 1, \dots, N_s$ ). This assumption is realistic since the sampling frequency is, in general, much larger than the mechanical vibration frequency. Introducing the  $(M \times N_s)$ -output matrix  $[\mathbf{Y}_{jk}] = [y_i(t_k)]$ , ( $i = 1, \dots, M$ ,  $k = 1, \dots, N_s$ ) and the  $(N \times N_s)$ -source matrix  $[\mathbf{S}_{jk}] = [s_j(t_k)]$ , the data model becomes

$$\mathbf{Y} = \mathbf{A}\mathbf{S}. \quad (5)$$

From (5), we have

$$\mathbf{Y}\mathbf{Y}^H = \mathbf{A}\mathbf{S}\mathbf{S}^H\mathbf{A}^H. \quad (6)$$

Provided that the number of samples is greater than the number of sources ( $N_s \geq N$ ),  $\mathbf{S}\mathbf{S}^H$  is full rank and the eigenvalue decomposition of  $\mathbf{Y}\mathbf{Y}^H$  yields

$$\mathbf{Y}\mathbf{Y}^H = \mathbf{U}_N \mathbf{\Lambda}_S \mathbf{U}_N^H \quad (7)$$

where  $\mathbf{\Lambda}_S$  is the diagonal matrix of the  $N$  nonnull eigenvalues of  $\mathbf{Y}\mathbf{Y}^H$ , and  $\mathbf{U}_N$  is the  $(M \times N)$  matrix of relevant eigenvectors.

The two previous expressions (6) and (7) lead us to seek the matrix  $\mathbf{A}$  such that

$$\mathbf{A} = \mathbf{U}_N \mathbf{W}. \quad (8)$$

The problem is now reduced to the estimation of the  $(N \times N)$  matrix  $\mathbf{W}$ .

Each entry of  $\mathbf{A}$  can be written as  $a_{ij} = \mathbf{u}_i^H \mathbf{w}_j$ , where  $\mathbf{u}_i^H$  is the  $i$ th row of  $\mathbf{U}_N$  and  $\mathbf{w}_j$  is the  $j$ th column of  $\mathbf{W}$ . Since each entry  $a_{ij}$  has the same modulus ( $= 1$ ), we can write

$$\|a_{ij}\|^2 = \mathbf{w}_j^H \mathbf{u}_i \mathbf{u}_i^H \mathbf{w}_j = 1, \quad \forall i, j. \quad (9)$$

From the different rows of  $\mathbf{U}_N$ , we form the  $M - 1$  matrices

$$\mathbf{K}_i = \mathbf{u}_{i+1} \mathbf{u}_{i+1}^H - \mathbf{u}_i \mathbf{u}_i^H, \quad i = 1, \dots, M - 1.$$

Considering the set of equations (9), we get

$$\mathbf{w}_j^H \mathbf{K}_i \mathbf{w}_j = 0, \quad \forall i, j.$$

The well-known property of the  $\text{vec}(\cdot)$  operator,<sup>1</sup>  $\text{vec}(\mathbf{ABC}) = (\mathbf{C}^T \otimes \mathbf{A})\text{vec}(\mathbf{B})$  (where  $\otimes$  is the Kronecker product), yields

$$\begin{aligned} \text{vec}(\mathbf{w}_j^H \mathbf{K}_i \mathbf{w}_j) &= (\mathbf{w}_j^T \otimes \mathbf{w}_j^H) \text{vec}(\mathbf{K}_i) \\ &= \text{vec}^T(\mathbf{K}_i)(\mathbf{w}_j \otimes \mathbf{w}_j^*) \\ &= 0, \quad \forall i, j. \end{aligned}$$

This set of equations is summarized by

$$\mathbf{K}(\mathbf{w}_j \otimes \mathbf{w}_j^*) = \mathbf{0}_{M-1}, \quad \forall j, \quad (10)$$

<sup>1</sup> $\text{vec}(\mathbf{X})$  is a concatenation of the columns of  $\mathbf{X}$ .

where  $\mathbf{K}$  is a  $((M - 1) \times N^2)$  matrix whose  $i$ th row is  $\text{vec}^T\{\mathbf{K}_i\}$  and  $\mathbf{0}_{M-1}$  is the  $(M - 1)$  null vector. Therefore, any vector  $(\mathbf{w}_j \otimes \mathbf{w}_j^*)$  is in the null space of  $\mathbf{K}$  denoted by  $\mathcal{N}\{\mathbf{K}\}$ .

REMARK 1 Equation (9) can be written as

$$\mathbf{P}(\mathbf{w}_j \otimes \mathbf{w}_j^*) = \mathbf{1}_M \quad (11)$$

where  $\mathbf{P}$  is a  $(M \times N^2)$  matrix whose  $i$ th row is  $\text{vec}^T\{\mathbf{u}_i \mathbf{u}_i^H\}$  and  $\mathbf{1}_M$  is the  $M$  vector of ones.

In the literature ([9, 12]), the solution of (11) is obtained thanks to a Householder matrix  $\mathbf{Q}$  such that

$$\mathbf{Q}\mathbf{P}(\mathbf{w}_j \otimes \mathbf{w}_j^*) = \lambda \mathbf{e}_1$$

where  $\mathbf{Q} = \mathbf{I}_M - 2\mathbf{q}\mathbf{q}^T/\mathbf{q}^T\mathbf{q}$  with  $\mathbf{q} = \mathbf{1}_M + \|\mathbf{1}_M\|\mathbf{e}_1$ , and  $\mathbf{e}_1 = [1, 0, \dots, 0]^T$ . Here, we made another choice,  $\mathbf{Q} = \mathbf{I}_M - \mathbf{1}_M \mathbf{e}_1^T$ , which yields the equation

$$\mathbf{Q}\mathbf{P}(\mathbf{w}_j \otimes \mathbf{w}_j^*) = \mathbf{0}_M.$$

The reason for this choice is that our method can be carried out on an antenna composed of identical paired sensors, instead of a set of omnidirectional sensors [14].

Since the matrix  $\mathbf{A}$  is full column rank according to (8), the vectors  $(\mathbf{w}_j \otimes \mathbf{w}_j^*)$ ,  $j \in \{1, \dots, N\}$  are linearly independent. If  $\dim\mathcal{N}\{\mathbf{K}\} = N$ , then, according to (10), those vectors span  $\mathcal{N}\{\mathbf{K}\}$ . The uniqueness of such a basis (i.e., with a Kronecker structure) is proved in Appendix A.

A necessary condition for having  $\dim\mathcal{N}\{\mathbf{K}\} = N$  is that matrix  $\mathbf{K}$  must contain  $N^2 - N$  independent columns, or at least  $N^2 - N$  rows. Consequently, the array must be composed of  $M \geq (N^2 - N + 1)$  sensors.

Since  $\dim\mathcal{N}\{\mathbf{K}\} = N$ , any vector  $\mathbf{b}_k \in \mathcal{N}\{\mathbf{K}\}$  can be decomposed as

$$\mathbf{b}_k = \sum_{j=1}^N \alpha_j (\mathbf{w}_j \otimes \mathbf{w}_j^*).$$

Performing the  $\text{vec}^{-1}(\cdot)$  operator on the previous equation, we get

$$\text{vec}^{-1}(\mathbf{b}_k) = \sum_{j=1}^N \alpha_j (\mathbf{w}_j^* \mathbf{w}_j^T) = \mathbf{W}^* \mathbf{\Sigma}_k \mathbf{W}^T \quad (12)$$

where  $\mathbf{\Sigma}_k = \text{diag}\{\alpha_1, \alpha_2, \dots, \alpha_N\}$ .

Then, we have the following proposition: It is always possible to find two vectors  $\mathbf{b}_1$  and  $\mathbf{b}_2$  such that the relevant diagonal matrices  $\mathbf{\Sigma}_1$  and  $\mathbf{\Sigma}_2$  satisfy the properties that  $\mathbf{\Sigma}_1$  is regular and  $\mathbf{\Sigma} = \mathbf{\Sigma}_1^{-1} \mathbf{\Sigma}_2$  has distinct diagonal entries.

Denoting  $\mathbf{R}_k \triangleq \text{vec}^{-1}(\mathbf{b}_k)$  and using (12) for  $k = 1, 2$ , we obtain

$$\mathbf{R}_1^{-1} \mathbf{R}_2 = \mathbf{W}^{-T} \mathbf{\Sigma} \mathbf{W}^T.$$

Since the diagonal entries of  $\mathbf{\Sigma}$  are all distinct, the identification of  $\mathbf{W}$  merges with the diagonalization of  $\mathbf{R}_1^{-1} \mathbf{R}_2$ .

Introducing the eigenvector matrix  $\mathbf{V}$  such that  $\mathbf{R}_1^{-1}\mathbf{R}_2 = \mathbf{V}\Sigma'\mathbf{V}^{-1}$ , the matrix  $\mathbf{W}$  corresponds to the inverse of the transposed matrix  $\mathbf{V}$ , except for a permutation and a complex factor.

Substituting  $\mathbf{W}$  by  $\mathbf{V}^{-T}$  in (8), and normalizing each column of  $\mathbf{U}_N\mathbf{V}^{-T}$  by the first term of each column, we obtain the matrix  $\mathbf{A}$ , except for an unknown permutation.

## B. Sensors Localization

1) *Calculation of DOAs ( $\theta_j$ ):* We consider  $\phi_{ij} \in [-\pi, \pi)$ , the phase of entry  $a_{ij}$  of the previously computed matrix  $\mathbf{A}$ . From (4), it follows that

$$\phi_{ij} = \frac{2\pi}{\lambda} \mathbf{p}_i^T \mathbf{n}_j.$$

Since the norm of the sensor 2 position vector is known and is lower than  $\lambda/2$ , and since the reference axis is chosen such that  $\mathbf{p}_2 = [\|\mathbf{p}_2\|, 0]^T$ , we get

$$\phi_{2j} = \frac{2\pi}{\lambda} \|\mathbf{p}_2\| \sin(\theta_j).$$

The DOAs are then given by

$$\theta_j = a \sin\left(\frac{\phi_{2j}\lambda}{2\pi\|\mathbf{p}_2\|}\right), \quad j = 1, \dots, N. \quad (13)$$

2) *Solving Phase Ambiguities and Sensor Localization ( $\mathbf{p}_i$ ):* Given  $\mathbf{p}_i^r$ , the at-rest position vector, and  $\mathbf{p}_i'$  the position relative to  $\mathbf{p}_i^r$ , the position vector  $\mathbf{p}_i$  can be broken down into

$$\mathbf{p}_i = \mathbf{p}_i^r + \mathbf{p}_i', \quad i > 2. \quad (14)$$

So, entry  $a_{ij}$  can be written as

$$a_{ij} = \exp\left(j\frac{2\pi}{\lambda}\mathbf{p}_i'^T\mathbf{n}_j\right) \exp\left(j\frac{2\pi}{\lambda}\mathbf{p}_i^{rT}\mathbf{n}_j\right), \quad i > 2.$$

Hence,

$$\exp\left(j\frac{2\pi}{\lambda}\mathbf{p}_i'^T\mathbf{n}_j\right) = a_{ij} \exp\left(-j\frac{2\pi}{\lambda}\mathbf{p}_i^{rT}\mathbf{n}_j\right), \quad i > 2. \quad (15)$$

We compute the argument of the right-hand side of the previous expression (denoted by  $\phi'_{ij}$ ) restricted to  $[-\pi, \pi)$ :

$$\phi'_{ij} = \arg\left\{a_{ij} \exp\left(-j\frac{2\pi}{\lambda}\mathbf{p}_i^{rT}\mathbf{n}_j\right)\right\}, \quad i > 2.$$

From (15), the relative positions  $\mathbf{p}_i'$  satisfy

$$\frac{2\pi}{\lambda}\mathbf{p}_i'^T\mathbf{n}_j = \phi'_{ij} + k_{ij}^\circ 2\pi, \quad i > 2 \quad \text{and} \quad k_{ij}^\circ \in \mathbb{Z}. \quad (16)$$

Equivalently, for any sources

$$\begin{bmatrix} \mathbf{n}_1^T \\ \vdots \\ \mathbf{n}_N^T \end{bmatrix} \mathbf{p}_i' = \frac{\lambda}{2\pi} \left( \begin{bmatrix} \phi'_{i1} \\ \vdots \\ \phi'_{iN} \end{bmatrix} + \begin{bmatrix} k_{i1}^\circ \\ \vdots \\ k_{iN}^\circ \end{bmatrix} 2\pi \right). \quad (17)$$

For sensor  $i$ , the scalar  $k_{ij}^\circ$  is the number of phase rotations between its current position  $\mathbf{p}_i$  and its at-rest position  $\mathbf{p}_i^r$  due to the  $j$ th source. For the large deformations we consider, the integers  $|k_{ij}^\circ|$  may not be zero.

We introduce the following notation:

$$\mathbf{C} \triangleq [\mathbf{n}_1^T, \dots, \mathbf{n}_N^T]^T, \quad \phi_i' \triangleq [\phi'_{i1}, \dots, \phi'_{iN}]^T, \quad \mathbf{k}_i \triangleq [k_{i1}, \dots, k_{iN}]^T \quad \text{and} \quad \mathbf{k}_i^\circ \triangleq [k_{i1}^\circ, \dots, k_{iN}^\circ]^T.$$

We now have to solve the general equation

$$\mathbf{C}\mathbf{p}_i'(\mathbf{k}_i) = \frac{\lambda}{2\pi}(\phi_i' + \mathbf{k}_i 2\pi), \quad i > 2 \quad (18)$$

where the unknowns are  $\mathbf{p}_i'(\mathbf{k}_i)$  and  $\mathbf{k}_i$ .

It is obvious that there are infinitely many solutions: all the solutions  $\mathbf{k}_i$  such that  $\mathbf{k}_i \in \mathbb{Z}^N$  and  $(\phi_i' + \mathbf{k}_i 2\pi) \in \text{range of } \mathbf{C}$ . In these conditions, the relevant solutions for  $\mathbf{p}_i'(\mathbf{k}_i)$  are given by

$$\mathbf{p}_i'(\mathbf{k}_i) = \frac{\lambda}{2\pi} \mathbf{C}^\# (\phi_i' + \mathbf{k}_i 2\pi). \quad (19)$$

The superscript  $\#$  denotes the Moore-Penrose pseudoinverse.

Nevertheless, physical considerations allow us to claim that the true solution  $\mathbf{k}_i^\circ$  lies in a finite subset of  $\mathbb{Z}^N$ , say  $\mathcal{D}$ . In the case of an airborne antenna,  $\|\mathbf{p}_i'\| \leq N_r \lambda$ , ( $N_r \in \mathbb{N}$ ) and consequently, from (16),  $\mathcal{D}$  reduces to

$$\begin{aligned} \mathcal{D} &= \underbrace{\{-N_r, \dots, N_r\} \times \dots \times \{-N_r, \dots, N_r\}}_{N \times} \\ &= \{-N_r, \dots, N_r\}^N. \end{aligned}$$

Now we make the following local observability assumption:  $\mathbf{k}_i^\circ$  is a unique vector  $\mathbf{k}_i \in \mathcal{D}$  such that  $(\phi_i' + \mathbf{k}_i^\circ 2\pi)$  is in the range of  $\mathbf{C}$ .

REMARK 2 Note that since the range of  $\mathbf{C}$  is  $2D$ , a necessary condition of uniqueness is that the number of sources is greater than 2. A sufficient condition is provided in Appendix B.

REMARK 3 To satisfy the local observability assumption, it may be necessary either to deal with a higher number of sources whenever it is possible, or to take into account additional physical considerations. For example, we can consider that the relative intersensor distance deformations are small (since we are in the case of an airborne antenna), i.e.,

$$\frac{\|\mathbf{p}_{i+1} - \mathbf{p}_i\| - \|\mathbf{p}_{i+1}^r - \mathbf{p}_i^r\|}{\|\mathbf{p}_{i+1}^r - \mathbf{p}_i^r\|} \leq \epsilon, \quad \forall i. \quad (20)$$

(16) So, infeasible calculated positions can be discarded.

TABLE I  
Phase Ambiguities Reduction Algorithm

Initiate the range ambiguity set $\mathcal{D}$ and the physical model criterion $\epsilon$
1) Select a vector $\mathbf{k}_i \in \mathcal{D}$
2) Compute $\mathbf{p}'_i(\mathbf{k}_i)$ according to (19) and $\mathbf{p}_i(\mathbf{k}_i)$ with (14)
3) if $(\phi'_i + \mathbf{k}_i 2\pi)$ is in the range of $\mathbf{C}$ , i.e., if $\mathbf{p}'_i(\mathbf{k}_i)$ and $\mathbf{k}_i$ satisfy
$\mathbf{C}^T \mathbf{p}'_i(\mathbf{k}_i) - \frac{\lambda}{2\pi} (\phi'_i + \mathbf{k}_i 2\pi) = 0 \quad (6)$
and if $\mathbf{p}_i(\mathbf{k}_i)$ verifies the physical constraints (20), then $\mathbf{k}_i^\circ = \mathbf{k}_i$ and $\mathbf{p}'_i(\mathbf{k}_i^\circ) = \mathbf{p}'_i$ , $\mathbf{p}_i(\mathbf{k}_i^\circ) = \mathbf{p}_i$ , else go to 1

To determine  $\mathbf{k}_i^\circ$ , we use the greedy algorithm as seen in Table I.

#### IV. SELF-CALIBRATION IN PRESENCE OF NOISE

##### A. Introduction

Now, let us consider the practical case where the recordings are corrupted by additive noise. Here, the sampled data model deduced from (3) becomes

$$\mathbf{y}(t_k) = \mathbf{A}(t_k) \mathbf{s}(t_k) + \boldsymbol{\eta}(t_k), \quad k = 1, \dots, N_s \quad (21)$$

and consequently, (6) is not valid anymore. Furthermore, the phase ambiguity solution presented in Table I of Section IIIB is particularly noise sensitive. The classical way to counteract noise effects is to increase the number of samples  $N_s$ . Consequently, due to the long observation time, one cannot ignore the time dependency of the array response matrix, and the previous direct method cannot be used.

For the applications and observation durations we deal with, the deformation of the antenna can be considered as the superposition of a large static bending (compared with the nominal shape) and low magnitude dynamic fluctuations due to vibrating modes, as shown in Fig. 2. We propose a two-step method based on a data model adapted to such a vibrating antenna. The aim of the first step is to solve the phase ambiguities  $\mathbf{k}_i^\circ$  from a long observation time. We only obtain an estimate of the static contribution of the array shape. In a second step, from a shorter observation time, we estimate an instantaneous array using the knowledge that there is no longer a phase ambiguity between the static and dynamic array shapes.

##### B. A Data Model Adapted to Vibrating Antennas

The position vector of the  $i$ th sensor is expressed as

$$\mathbf{p}_i(t) = \bar{\mathbf{p}}_i + \tilde{\mathbf{p}}_i(t) \quad (22)$$

where  $\bar{\mathbf{p}}_i = [\bar{x}_i, \bar{z}_i]^T$  is the static position vector and  $\tilde{\mathbf{p}}_i(t)$  is the dynamic position vector with a null temporal average.

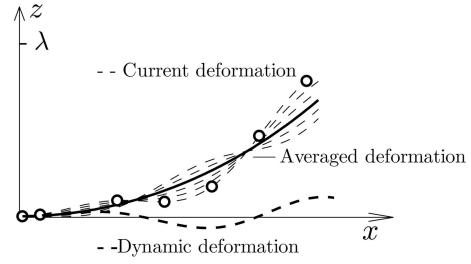


Fig. 2. Array shape dynamic model.

Substituting the position vector by its decomposition in (4), the entries of matrix  $\mathbf{A}(t)$  become

$$a_{ij}(t) = \exp \left\{ j \frac{2\pi}{\lambda} \bar{\mathbf{p}}_i^T \mathbf{n}_j \right\} \exp \left\{ j \frac{2\pi}{\lambda} \tilde{\mathbf{p}}_i^T(t) \mathbf{n}_j \right\} \\ \triangleq \bar{a}_{ij} \tilde{a}_{ij}(t).$$

In matrix notation, we write

$$\mathbf{A}(t) = \bar{\mathbf{A}} \circ \tilde{\mathbf{A}}(t) \quad (23)$$

where  $\circ$  represents Hadamard (element-wise) matrix multiplication.

Assuming that the dynamical distortions have low magnitude, the entries of the dynamical array response matrix  $\tilde{\mathbf{A}}(t)$  can be approximated by a first-order Taylor-series expansion:

$$\tilde{a}_{ij}(t) \stackrel{1}{=} 1 + j \frac{2\pi}{\lambda} \underbrace{\tilde{\mathbf{p}}_i^T(t) \mathbf{n}_j}_{f_{ij}(t)}$$

where the symbol  $\stackrel{1}{=}$  stands for a first-order approximation. In matrix notation,

$$\tilde{\mathbf{A}}(t) \stackrel{1}{=} \mathbf{1} + \mathbf{F}(t).$$

$\mathbf{1}$  is the  $M \times N$  ones matrix such that  $\mathbf{1}_{ij} = 1, \forall i, j$ .  $\mathbf{F}(t)$  only accounts for first-order time-dependent terms.

The first-order approximation can be done only if

$$\left| \frac{2\pi}{\lambda} \tilde{\mathbf{p}}_i^T(t) \mathbf{n}_j \right| \ll 1 \quad (24)$$

or

$$\frac{2\pi}{\lambda} \|\tilde{\mathbf{p}}_i(t)\| |\cos(\tilde{\mathbf{p}}_i(t), \mathbf{n}_j)| \ll 1.$$

A sufficient condition to validate the inequality (24)  $\forall j$  is

$$\|\tilde{\mathbf{p}}_i(t)\| \ll \frac{\lambda}{2\pi}. \quad (25)$$

Hence, (23) can be expressed by

$$\mathbf{A}(t) \stackrel{1}{=} \bar{\mathbf{A}} + \mathbf{D}(t) \quad (26)$$

where  $\mathbf{D}(t) \triangleq \bar{\mathbf{A}} \circ \mathbf{F}(t)$  is the time-dependent deviation matrix.

Substituting  $\mathbf{A}(t)$  using (26) into (3), we have

$$\mathbf{y}(t) = [\bar{\mathbf{A}} + \mathbf{D}(t)]\mathbf{s}(t) + \boldsymbol{\eta}(t). \quad (27)$$

This is our new data model adapted for vibrating antennas.

### C. A Two-Step Scales Method for Self-Calibration in Presence of Noise

#### 1) *First Step-Estimation of Static Array Shape:*

From (27), the new sampled data model becomes

$$\mathbf{y}(t_k) = [\bar{\mathbf{A}} + \mathbf{D}(t_k)]\mathbf{s}(t_k) + \boldsymbol{\eta}(t_k). \quad (28)$$

Let us compute the following matrix

$$\mathbf{R}_y \triangleq \frac{1}{N_s} \sum_{k=1}^{N_s} \mathbf{y}(t_k) \mathbf{y}^H(t_k).$$

From (28), we obtain

$$\begin{aligned} \mathbf{R}_y &= \bar{\mathbf{A}} \mathbf{R}_s \bar{\mathbf{A}}^H + \frac{1}{N_s} \sum_{k=1}^{N_s} D(t_k) s(t_k) s^H(t_k) D^H(t_k) \\ &\quad + \frac{1}{N_s} \sum_{k=1}^{N_s} \boldsymbol{\eta}(t_k) \boldsymbol{\eta}^H(t_k) + \mathbf{T}(N_s) \end{aligned} \quad (29)$$

where the matrix  $\mathbf{T}(N_s)$  collects all the cross-terms, and  $\mathbf{R}_s \triangleq (1/N_s) \sum_{k=1}^{N_s} s(t_k) s^H(t_k)$ .

Since  $\mathbf{R}_y$  is computed with a high number of samples (long observation time), it is important to study the asymptotic behavior of the previous equation.

When  $N_s \rightarrow \infty$ , we simultaneously have:

- 1)  $\bar{\mathbf{A}} \mathbf{R}_s \bar{\mathbf{A}}^H \rightarrow \bar{\mathbf{A}} \mathbf{E}\{\mathbf{s}\mathbf{s}^H\} \bar{\mathbf{A}}^H$  (where  $\mathbf{E}\{\cdot\}$  is the expectation operator) because of the ergodicity and stationarity properties of the sources,
- 2)  $(1/N_s) \sum_{k=1}^{N_s} D(t_k) s(t_k) s^H(t_k) D^H(t_k) \rightarrow$  constant matrix depending on the magnitude of the vibrations (see Appendix C),
- 3)  $(1/N_s) \sum_{k=1}^{N_s} \boldsymbol{\eta}(t_k) \boldsymbol{\eta}^H(t_k) \rightarrow \eta^2 \mathbf{I}_M$  (where  $\mathbf{I}_M$  is the  $(M \times M)$  identity matrix) because of the statistical properties of the noise,
- 4)  $\mathbf{T}(N_s) \rightarrow 0$ , as shown in Appendix C.

Hence, for the long observation time we consider here,  $\mathbf{R}_y$  reduces to

$$\mathbf{R}_y = \bar{\mathbf{A}} \mathbf{R}_s \bar{\mathbf{A}}^H + \underbrace{\frac{1}{N_s} \sum_{k=1}^{N_s} D(t_k) s(t_k) s^H(t_k) D^H(t_k)}_{\text{2nd order matrix}} + \eta^2 \mathbf{I}_M. \quad (30)$$

Moreover, if the vibration's magnitudes are small (see (25)), the second-order matrix of the previous equation can be neglected and we finally obtain

$$\mathbf{R}_y \stackrel{1}{=} \bar{\mathbf{A}} \mathbf{R}_s \bar{\mathbf{A}}^T + \eta^2 \mathbf{I}_M. \quad (31)$$

As in Section IIIA, the estimation of  $\bar{\mathbf{A}}$  is inspired by the methods described in [12] and [9]. Since  $\mathbf{R}_s$  is a  $(N \times N)$  regular matrix, the eigenvalue decomposition of  $\mathbf{R}_y$  can be written as

$$\mathbf{R}_y = \mathbf{U} \begin{bmatrix} \Lambda_s & 0 \\ 0 & 0 \end{bmatrix} \mathbf{U}^H + \eta^2 \mathbf{U} \mathbf{U}^H. \quad (32)$$

$\Lambda_s + \eta^2 \mathbf{I}_N$  is the diagonal matrix containing the  $N$  largest eigenvalues of  $\mathbf{R}_y$ . Denoting  $\mathbf{U}_N$  as the matrix of eigenvectors corresponding to the  $N$  largest eigenvalues of  $\mathbf{R}_y$ , the matrix  $\bar{\mathbf{A}}$  has the structure  $\bar{\mathbf{A}} = \mathbf{U}_N \mathbf{W}$ , and can be hence estimated by using CMA as described in Section IIIA.

Then, from this matrix  $\bar{\mathbf{A}}$ , we use the method developed in Section IIIB, substituting the position vector  $\mathbf{p}_i$  by  $\bar{\mathbf{p}}_i$ .

First, we estimate the DOAs  $\theta_j$  according to (13).

Second, the vector of phase rotations  $\mathbf{k}_i^\circ$  between  $\bar{\mathbf{p}}_i$  and  $\mathbf{p}_i^r$  is found as

$$\mathbf{k}_i^\circ = \min_{\mathbf{k}_i \in \mathcal{D}} \left\| \mathbf{C}^T \mathbf{p}_i'(\mathbf{k}_i) - \frac{\lambda}{2\pi} (\phi_i' + \mathbf{k}_i 2\pi) \right\| \quad (33)$$

instead of (6) in the greedy algorithm.

Finally, the static array shape is given by

$$\bar{\mathbf{p}}_i = \mathbf{p}_i^r + \mathbf{p}_i'. \quad (34)$$

An instantaneous shape can be obtained with the following second step.

2) *Second-Step. Estimation of Dynamic Array Shape:* This step estimates the current position  $\mathbf{p}_i(t_k)$  ( $\forall k = 1, \dots, N_s$ ) from the knowledge of the static position  $\bar{\mathbf{p}}_i$  estimated in Step 1. The relative deformation between the estimated static array and the actual one is small, i.e., always smaller than half the wavelength, and there is no phase rotation. Hence, the very noise-sensitive stage to find the phase rotation number (see (6) in Table I) is no longer necessary. So it is possible to reduce the number of samples down to  $N_d$  ( $N_d \ll N_s$ ) to satisfy the local time independence, i.e.,  $\mathbf{p}_i(t_l) = \mathbf{p}_i(t_k)$ ,  $l \in \{k, \dots, k + N_d\}$ ; therefore,  $\mathbf{A}$  is a constant piecewise matrix  $\mathbf{A}(t_l) = \mathbf{A}(t_k)$ ,  $l \in \{k, \dots, k + N_d\}$ .

The data model yields

$$\mathbf{y}(t_l) = \mathbf{A}(t_k) \mathbf{s}(t_l) + \boldsymbol{\eta}(t_l), \quad l = k, \dots, k + N_d. \quad (35)$$

At each time  $t_k$ , the matrix  $\mathbf{A}(t_k)$  is obtained by performing a CMA (8)–(13) on  $\mathbf{R}_y(t_k)$ , where

$$\mathbf{R}_y(t_k) = \frac{1}{N_d} \sum_{l=k}^{k+N_d} \mathbf{y}(t_l) \mathbf{y}^H(t_l). \quad (36)$$

Now, let us compute the argument  $\phi_{ij}(t_k)$  of an entry  $a_{ij}(t_k)$  of  $\mathbf{A}(t_k)$ . This argument satisfies

$$\phi_{ij}(t_k) + k_{ij}^\circ 2\pi = \frac{2\pi}{\lambda} \mathbf{p}_i^T(t_k) \mathbf{n}_j.$$

TABLE II  
Direct Large Array Shape Self-Calibration Algorithm

---

**Step 1:** Static array shape estimation (see Section IVC1)

- 1.1) Estimate  $\bar{\mathbf{A}}$  from  $\mathbf{R}_y$  computed with  $N_s$  samples, see Section IIIA
- 1.2) Estimate the DOAs  $\boldsymbol{\theta} = [\theta_1, \dots, \theta_N]^T$ , (13)
- 1.3) Determine the phase rotation number vector  $\{\mathbf{k}_i^\circ\}_{i=3}^M$  between  $\{\mathbf{p}_i^r\}_{i=3}^M$  and  $\{\bar{\mathbf{p}}_i\}_{i=3}^M$  from the greedy algorithm of Section IIIB using the criterion (33)
- 1.4) Estimate the static sensor locations  $\{\bar{\mathbf{p}}_i\}_{i=3}^M$ , using (34)

**Step 2:** Dynamic array shape estimation (see Section IVC2)

Set  $k = 1$

- 2.1) Estimate  $\mathbf{A}(t_k)$  from  $\mathbf{R}_y(t_k)$  computed on  $N_d$  samples, see Section IIIA
- 2.2) Estimate  $\{\tilde{\mathbf{p}}_i(t_k)\}_{i=3}^M$  from  $\{\bar{\mathbf{p}}_i\}_{i=3}^M$  and  $\boldsymbol{\theta}$ , using (37)
- 2.3) Sensor's location estimation  $\{\mathbf{p}_i(t_k)\}_{i=3}^M$ , using (22)

Set  $k = k + 1$   
go back to 2.1 until  $k = N_s - N_d$

---

Then, let us compute the argument  $\bar{\phi}_{ij}$  of an entry of  $\bar{\mathbf{A}}$  of Step 1. We still have

$$\bar{\phi}_{ij} + k_{ij}^\circ 2\pi = \frac{2\pi}{\lambda} \bar{\mathbf{p}}_i^T \mathbf{n}_j.$$

Since the number of phase rotations  $k_{ij}^\circ$  is the same in the two previous equations, thanks to (22), the dynamic position  $\tilde{\mathbf{p}}_i(t_k) = \mathbf{p}_i(t_k) - \bar{\mathbf{p}}_i$  satisfies

$$\mathbf{n}_j^T \tilde{\mathbf{p}}_i(t_k) = \frac{\lambda}{2\pi} [\phi_{ij}(t_k) - \bar{\phi}_{ij}], \quad i > 2.$$

From the set of sources, the dynamical positions  $\tilde{\mathbf{p}}_i(t_k)$  can then be computed with

$$\tilde{\mathbf{p}}_i(t_k) = \frac{\lambda}{2\pi} \begin{bmatrix} \mathbf{n}_1^T \\ \vdots \\ \mathbf{n}_N^T \end{bmatrix}^\# \begin{bmatrix} \phi_{i1}(t_k) - \bar{\phi}_{i1} \\ \vdots \\ \phi_{iN}(t_k) - \bar{\phi}_{iN} \end{bmatrix}. \quad (37)$$

Finally,  $\bar{\mathbf{p}}_i$  and  $\tilde{\mathbf{p}}_i(t_k)$  being known, the current position vector  $\mathbf{p}_i(t_k)$  can be obtained for any sensor  $i$  at time  $t_k$  using (22).

#### D. Algorithms

The two time scale previous method is summarized in Table II.

**REMARK 4** Practically, the available number of samples  $N_s$  does not allow the matrix  $\mathbf{T}(N_s)$  to be neglected in the expression of  $\mathbf{R}_y$  in (29). Moreover the inequality (25) is not strong enough to ensure that the second-order terms in (30) will be negligible. So the matrix obtained in Step 1.1 of the previous algorithm is only a coarse version of  $\bar{\mathbf{A}}$ , denoted by  $\hat{\bar{\mathbf{A}}}$ . Consequently, Step 1.2 yields to a biased estimation of the DOAs  $\boldsymbol{\theta}$ . This error is sufficiently small so that the estimation of the numbers of phase rotations remains valid in Step 1.3. Equivalently, the coarse array

TABLE III  
Iterative Large Array Shape Self-Calibration Algorithm

---

**Step 1:** Coarse static array shape estimation (see Section IVC1)

- 1.1) Estimate  $\bar{\mathbf{A}}$  from  $\mathbf{R}_y$  computed with  $N_s$  samples (see Section IIIA)
- 1.2) Estimate DOAs  $\boldsymbol{\theta}^{(0)}$  using (13)
- 1.3) Determine the phase rotation number vector  $\{\mathbf{k}_i^\circ\}_{i=3}^M$  between  $\{\mathbf{p}_i^r\}_{i=3}^M$  and  $\{\bar{\mathbf{p}}_i\}_{i=3}^M$  from (33)
- 1.4) Estimate the biased static sensor locations  $\{\hat{\bar{\mathbf{p}}}_i\}_{i=3}^M$ , using (34)

**Step 2:** Iterative bias reduction—Estimation of the dynamic array shape

Set  $k = 1$

- 2.1) Estimate  $\mathbf{A}(t_k)$  from  $\mathbf{R}_y(t_k)$  computed on  $N_d$  samples; see Section IIIA
- 2.2) Estimate DOAs  $\hat{\boldsymbol{\theta}}$ , using (13)
- 2.3) Refine DOAs using  $\boldsymbol{\theta}^{(k)} = (1/(k+1))(\hat{\boldsymbol{\theta}} + k\boldsymbol{\theta}^{(k-1)})$
- 2.4) Estimate  $\{\tilde{\mathbf{p}}_i(t_k)\}_{i=3}^M$  from  $\{\hat{\bar{\mathbf{p}}}_i\}_{i=3}^M$  and  $\boldsymbol{\theta}^{(k)}$ , using (37)

Set  $k = k + 1$   
go back to 2.1 until  $k = N_s - N_d$

- 2.5) Estimate the final sensor's location  $\{\mathbf{p}_i(t_{N_s - N_d})\}_{i=3}^M$ , using (22)

---

shape obtained  $\{\hat{\bar{\mathbf{p}}}_i\}_{i=3}^M$  is a biased but nonambiguous estimate.

Since the DOAs are time independent, it is possible to iteratively refine the DOA estimates during Step 2 to iteratively unbiased the dynamical position  $\mathbf{p}_i(t_k)$ .

Of course, with a backward iterative procedure, it is always possible to unbiased the static positions as well.

Based on previous considerations, we propose the algorithm as seen in Table III.

Only this last algorithm is used in our numerical simulations.

## V. EXTENSION TO DUAL-BAND SENSOR ARRAYS

### A. Contribution of Dual-Band Sensors

Our algorithms allow us to self-calibrate arrays composed of at least  $M = N^2 - N + 1$  sensors. As we noted in Remark 3 of Section IIIB, the number of ambiguous solution decreases as the number of available sources increases. Practically, the necessary number of sensors quickly becomes prohibitive. One way to deal with a higher number of sources while maintaining the same number of sensors is to use multi-band sensors.

As an example, with our method, when the 2D problem of large array shape self-calibration is considered, at least 3 sources are necessary (Remark 2). The minimum number of sensors must then be equal to 7 for a single carrier frequency case, but only 3 dual-band sensors are needed with two carrier frequencies.

## B. Algorithm Extension to Dual-Band Sensors

The extension to dual-band sensors case is straightforward. In fact we have to deal with two independent records

$$\mathbf{y}^1(t) = \mathbf{A}^1(t)\mathbf{s}^1(t) + \boldsymbol{\eta}^1(t)$$

$$\mathbf{y}^2(t) = \mathbf{A}^2(t)\mathbf{s}^2(t) + \boldsymbol{\eta}^2(t)$$

where the superscripts <sup>1</sup> and <sup>2</sup> are used to distinguish the two different wavelengths  $\lambda^1$  and  $\lambda^2$ . The estimation of the two array response matrices  $\mathbf{A}^1(t)$  and  $\mathbf{A}^2(t)$  is separately performed using CMA on each relevant recording (Steps 1.1 and 2.1 of previous algorithms). The others steps of the algorithms are performed with the whole phases obtained from the two wavelengths.

## VI. NUMERICAL SIMULATIONS

Our algorithm is tested on a large antenna (6 m) subjected to large deformations such that their magnitude at the tip of the array reaches 0.6 m. The source signals are generated by a Gaussian number random generator. For each simulation, white Gaussian noise is added under different signal-to-noise ratio (SNR), defined as  $\text{SNR} = 10\log_{10}(\sigma^2/\eta^2)$  where  $\sigma^2$  is the power of one source on a sensor and  $\eta^2$  is the noise power (the same on each sensor). The output signals are sampled at 60 kHz. Monte Carlo experiments are performed with 200 runs. The performance of our algorithm is compared with the CRLB. We also plot the corresponding 90% confidence ellipse.

### A. Case I. Large Deformation of a Static Antenna—Single Carrier Frequency Sources

The array is composed of  $M = 13$  omnidirectional sensors. Only the two first sensors are  $\lambda/2$  apart. At rest, the coordinates  $\mathbf{p}_i^r$  of the sensor  $i$  are

$$\mathbf{p}_i^r = \frac{\lambda}{2} \begin{bmatrix} 0 & 1 & 5 & 7 & 13 & 17 & 20 & 26 & 29 & 31 & 35 & 38 & 40 \\ 0 & & & & & & & \dots & & & & & 0 \end{bmatrix}.$$

We assume only a large static distortion without vibration phenomena (Fig. 3). At the tip of the array, the magnitude of the antenna's distortion reaches  $2\lambda$ ; hence, 6 sensors (sensors 8 to 13) have an “ambiguous location.” Three sources are impinging the array with the same wavelength  $\lambda = 0.3$  m. The DOAs are  $\boldsymbol{\theta} = [-36^\circ, 3^\circ, 20^\circ]$ . The SNR is equal to 40 dB.

Fig. 4 presents the self-calibration result at the end of Step 1 without the resolution of phase ambiguities using  $N_s = 7500$  samples. As a consequence, the rightmost six sensor positions are not correctly estimated.

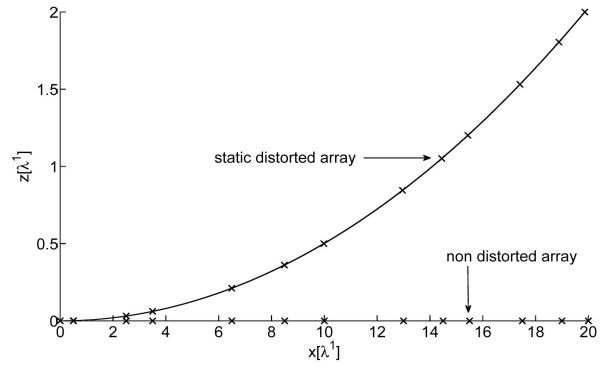


Fig. 3. Simulated array with static distortion only.

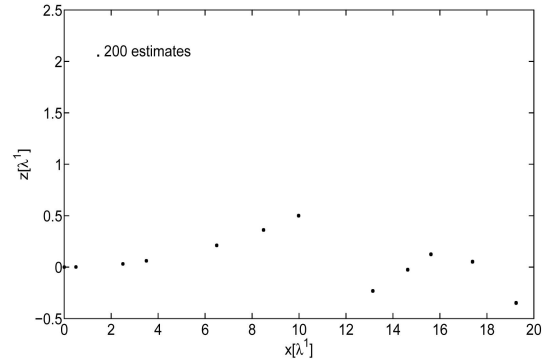


Fig. 4. 200 static bending estimates without resolution of phase ambiguities.

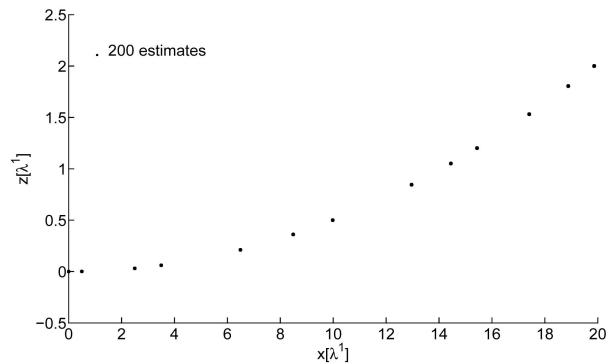


Fig. 5. 200 static bending estimates.

Fig. 5 presents the Step 1 result using the phase ambiguity resolution procedure (see Table I of Section IIIB) inside the range ambiguities  $\mathcal{D} = \{-2, -1, 0, 1, 2\}^3$ , completed by the physical model (20) with  $\epsilon = 0.1$ . We notice that all of the phase ambiguities have been resolved. Fig. 6 focuses on the rightmost sensor. We compare the results with a 90% confidence ellipse computed from the CRLB presented in [8].

Table IV details the bias and standard deviation of the location estimates of the rightmost sensor. The square root of the CRLB is also provided.

We can see that the estimation procedure is almost efficient.

TABLE IV  
Performance of the 200 Rightmost Sensor Localizations

Unit = $10^{-3}\lambda$	Bias	STD	$\sigma_{\text{CRB}}$
$x$	-0.065	1.647	1.223
$z$	-0.003	0.633	0.557

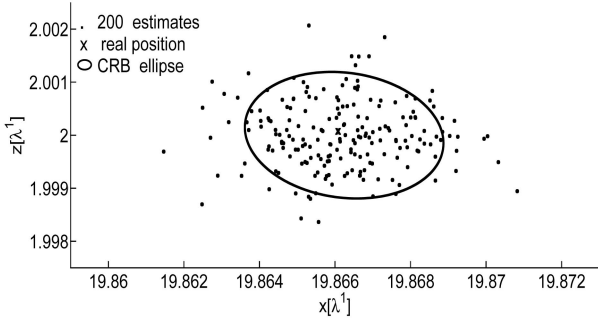


Fig. 6. Focus on 200 estimates of location of rightmost sensor and 90% ellipse based on CRLB.

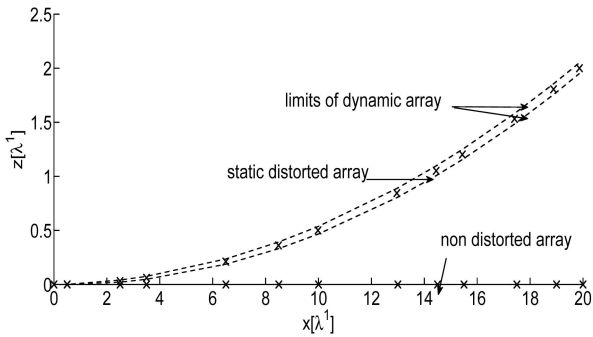


Fig. 7. Array at rest and with deformations (static+dynamic).

### B. Case II. Large Deformation of a Vibrating Antenna—Single Carrier Frequency Sources

In this subsection, the array, the static deformation, the DOAs and the SNR are the same as the previous subsection. Here, the array is subject to a 2 Hz vibrating mode presented via the dotted line in Fig. 7. The node is on the first sensor, and the anti-node on the rightmost sensor has a  $0.05\lambda$  magnitude. For Step 1, we take  $N_s = 7500$ , and for Step 2, we take  $N_d = 300$ .

Figs. 8 and 9 present the results at the end of Step 1 (static shape estimation) using the phase ambiguity resolution procedure with  $\mathcal{D} = \{-2, -1, 0, 1, 2\}^3$  and  $\epsilon = 0.1$ .

Fig. 9 focuses on the location estimates of the rightmost sensor. It illustrates a localization bias ( $16.77 \cdot 10^{-3}\lambda$  for  $x$ ,  $30.67 \cdot 10^{-3}\lambda$  for  $z$ ). As we said in Remark 4, this bias is due to the presence of nonnegligible 2nd-order terms in the matrix in  $\mathbf{R}_y$ . Nevertheless, there are no ghost positions the static shape estimates.

Note that the position obtained at the end of Step 1 is used in Step 2 initialization. Fig. 10 presents the

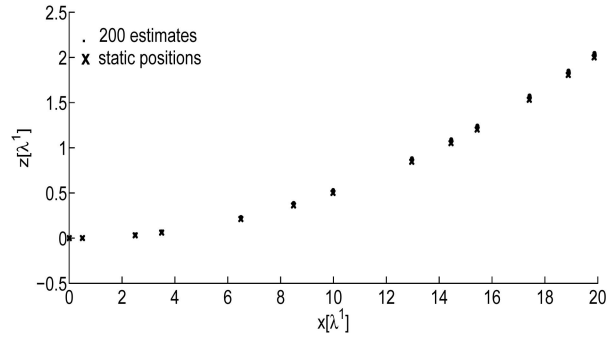


Fig. 8. 200 estimates of static bending.

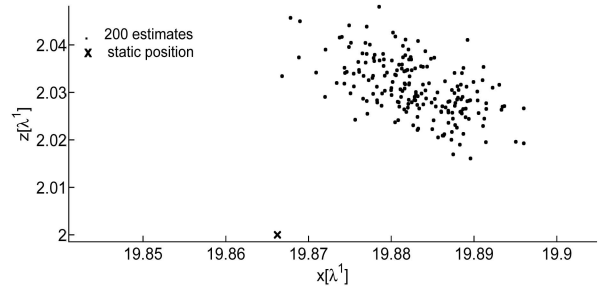


Fig. 9. Focus on 200 estimates of estimates of location of rightmost sensor.

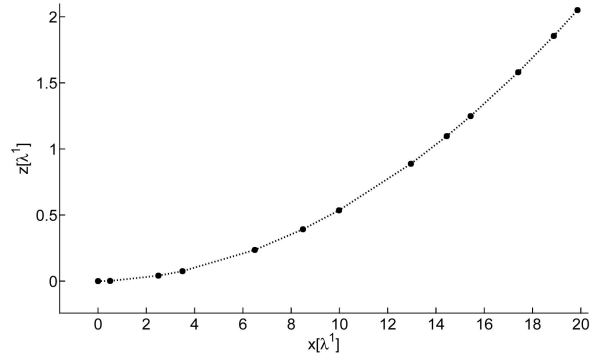


Fig. 10. 200 estimates of array shape.

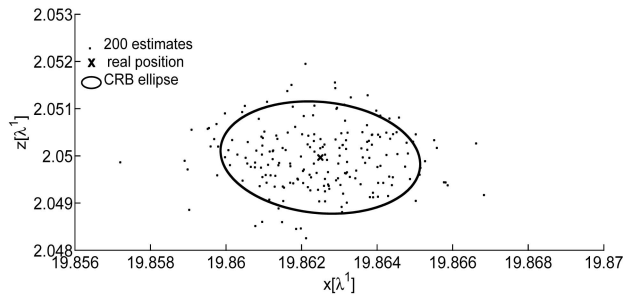


Fig. 11. Focus 200 estimates of location of rightmost sensor and confidence ellipse.

final results for the 200 runs. Fig. 11 focuses on the estimated position of the 13th sensor, which is the most difficult to locate.

The elements of the CRLB corresponding to sensor position are greater when the sensors move than when they are motionless. Because we do not

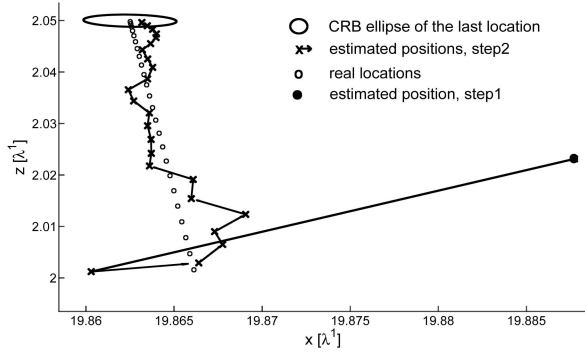


Fig. 12. Step 2 intermediate results and confidence ellipse for 13th sensor final position.

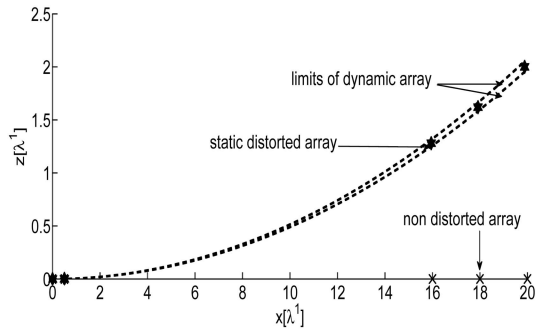


Fig. 13. Simulated 5-sensor array at rest and with deformations.

have any model for this motion, we use the CRLB computed for the static case as reference.

Bias and standard deviation for the location estimates of the 13th sensor are detailed in Table V. The square root of the CRLB is also provided for comparison.

We can see that this two-step method leads to an unbiased location estimate of the rightmost sensor. Compared with the static CRLB one can say the method remains almost efficient.

Fig. 12 presents an example of iterative localization performed by Step 2. One can see the improvement of the location estimate at each iteration. Table VI exposes the performance of the iterative algorithm for different SNRs. We consider the bias, the standard deviation, and the square root of the CRLB for the estimation of the final position of the 13th sensor. One can see the statistical efficiency of our method, even for a low SNR.

### C. Case III. Large Deformation and Vibrating Antenna—Dual-Band Sensors

In this subsection, the array and the deformations are the same as in Subsection VIB. However, here we consider sources of different wavelengths,  $\lambda^1 = 0.3$  m and  $\lambda^2 = 0.5$  m. There are 3 sources associated with each wavelength. The DOAs are  $\theta^1 = \theta^2 = [-36^\circ, 3^\circ, 20^\circ]$  for each relevant wavelength.

TABLE V

Performance of the 200 Estimates of the Rightmost Sensor at the End of Step 2

Unit = $10^{-3}\lambda$	Bias	STD	$\sigma_{\text{CRB}}$
x	-0.040	1.636	1.232
z	-0.009	0.649	0.554

TABLE VI

Performance of the 200 Rightmost Sensor Localizations According to Various SNR

Unit = $10^{-3}\lambda$	20 dB	30 dB	40 dB
Bias x	-0.569	-0.198	-0.040
Bias z	-0.031	-0.022	-0.009
STD x	16.42	5.175	1.636
$\sigma_{\text{CRB}}$ x	12.32	3.895	1.232
STD z	6.343	1.984	0.649
$\sigma_{\text{CRB}}$ z	5.547	1.754	0.554

TABLE VII

Performance of 200 Location Estimates for the Rightmost Sensor using Dual-Band Sensors

Unit = $10^{-3}\lambda$	0 dB	10 dB	20 dB	30 dB	40 dB
Bias x	15.84	3.979	1.259	0.418	0.156
Bias z	-0.970	-1.177	-0.439	-0.143	-0.043
STD x	135.1	41.05	12.95	4.103	1.310
$\sigma_{\text{CRB}}$ x	100.5	31.14	9.828	3.101	0.983
STD z	56.61	17.56	5.569	1.769	0.579
$\sigma_{\text{CRB}}$ z	46.14	14.11	4.445	1.405	0.444

TABLE VIII

Unsolved Phase Ambiguity (%) SNR = 10 dB

%	$\epsilon = \infty$	$\epsilon = 0.1$
Mono-sensor	70%	1.5%
Dual-sensor	1%	0%

Table VII shows the performance, according to various SNR, compared with the square root of the corresponding CRLB. The algorithm remains almost efficient, and even allows us to deal with low SNRs (10 dB and 0 dB).

Table VIII gives the percentage of unsuccessful location estimates arising from unresolved phase ambiguities between several cases: mono- and dual-sensors, coupled, or not, to physical constraints. Here we have SNR = 10 dB. Robustness increases when dual sensors are coupled to physical constraint.

### D. Case IV. Large Deformations of a Vibrating, Sparse Dual-Band Array

This section studies the self-calibration of sparse array composed of only  $M = 5$  sensors (Fig. 13). At

TABLE IX  
Performance of the 200 Dual-Band Rightmost Sensor  
Localizations

Unit = $10^{-3}\lambda^1$	10 dB	20 dB	30 dB	40 dB
Bias x	2.284	1.105	0.407	0.156
Bias z	-0.821	-0.188	-0.045	-0.006
STD x	55.82	17.65	5.615	1.818
$\sigma_{\text{CRB}}$ x	50.01	15.81	4.999	1.581
STD z	20.78	6.471	2.036	0.647
$\sigma_{\text{CRB}}$ z	18.62	5.848	1.848	0.584

rest, the sensor coordinates are

$$\mathbf{p}^r = \frac{\lambda^1}{2} \begin{bmatrix} 0 & 1 & 32 & 36 & 40 \\ 0 & 0 & 0 & 0 & 0 \end{bmatrix}.$$

The different wavelengths are  $\lambda^1 = 0.3$  m and  $\lambda^2 = 0.5$  m. There are 2 sources in each band. The DOAs are, respectively,  $\theta^1 = [-36^\circ, 3^\circ]$  and  $\theta^2 = [-6^\circ, 16^\circ]$ .

Performance according to various SNRs and comparisons with the square root of the corresponding CRB are given in Table IX.

## VII. CONCLUSION

This paper presented a new, almost efficient method for self-calibrating large distorted and vibrating antennas using noncooperating narrowband sources. The estimation of the different array response matrices (static and dynamic) is based on an original formulation of the CMA. Then, we study and solve the phase ambiguities arising from the large distortions to provide a coarse estimate of the static array shape. Finally, the missing phase rotation numbers are estimated, and the same are iteratively processed to obtain an almost efficient estimate of array position.

## APPENDIX A

In the subspace  $\mathcal{N}\{\mathbf{K}\}$ , any vector of the form  $\mathbf{v} \otimes \mathbf{v}^*$  can be written as

$$\mathbf{v} \otimes \mathbf{v}^* = \sum_{j=1}^N \gamma_j \mathbf{w}_j \otimes \mathbf{w}_j^*.$$

We can equivalently rearrange this vector decomposition in terms of matrices of rank 1 using the  $\text{vec}^{-1}(\cdot)$  operator:

$$\text{vec}^{-1}(\mathbf{v} \otimes \mathbf{v}^*) = \mathbf{v}^* \mathbf{v}^T = \sum_{j=1}^N \gamma_j \mathbf{w}_j \mathbf{w}_j^T.$$

Since all the matrices involved have rank 1, all coefficients  $\gamma_j$  are zero except for one. Consequently,

any vector structured as  $\mathbf{v} \otimes \mathbf{v}^* \in \mathcal{N}\{\mathbf{K}\}$  is necessarily collinear to one of the vectors  $\mathbf{w}_j \otimes \mathbf{w}_j^*$ . We can then claim that  $\mathbf{W}$  is unique, except for a permutation and a scaling factor over its columns.

## APPENDIX B

From a true position  $\mathbf{p}_i$ , let us consider a nonobservable shift  $\Delta \mathbf{p}_i$ , i.e.,

$$\exp \left\{ j \frac{2\pi}{\lambda} (\mathbf{p}_i^T + \Delta \mathbf{p}_i^T) \mathbf{n}_j \right\} = a_{ij}, \quad \forall j.$$

From  $a_{ij} = \exp\{j(2\pi/\lambda)\mathbf{p}_i^T \mathbf{n}_j\}$ ,

$$\frac{2\pi}{\lambda} \Delta \mathbf{p}_i^T \mathbf{n}_j = \Delta k_{ij} 2\pi, \quad \forall j. \quad (38)$$

We can write

$$k_{ij} = k_{ij}^\circ + \Delta k_{ij}, \quad \forall j$$

where  $k_{ij}$  is the phase rotation parameter we use in the greedy algorithm of Section III B, and  $k_{ij}^\circ$  denotes the phase rotation number corresponding to the true sensor  $i$  position. Because of physical considerations,  $k_{ij}$  is searched in the finite domain  $\mathcal{D} = \{-N_r, \dots, N_r\}^N$ .

It is interesting to rewrite (38) as

$$\frac{1}{\lambda} \|\Delta \mathbf{p}_i\| \cos(\mathbf{n}_j, \Delta \mathbf{p}_i) = \Delta k_{ij}, \quad \forall j = \{1, \dots, N\}.$$

Since the DOAs  $\mathbf{n}_j$  are distinct by assumption and the function cosine is even, it is clear that it is impossible to have more than two identical  $\Delta k_{ij}$ . As a consequence, since  $\#\{\mathcal{D}\} = 2N_r + 1$ , when  $N > 4N_r + 2$ , all the  $k_{ij}$  cannot be in  $\mathcal{D}$ , and the problem is locally observable.

## APPENDIX C

Each entry  $y_i(t_k)$  of the vector  $\mathbf{y}(t_k)$  is given by

$$y_i(t_k) = \sum_{i'} (\bar{a}_{ii'} + d_{ii'}(t_k)) s_{i'}(t_k) + \eta_i(t_k) \quad (39)$$

where  $\bar{a}_{ii'}$  and  $d_{ii'}(t_k)$  are the entries of matrices  $\bar{\mathbf{A}}$  and  $\mathbf{D}(t_k)$ . While  $s_{i'}(t_k)$  is a realization of a random signal, assumed to be stationary and ergodic,  $d_{ii'}(t_k)$  is a deterministic time-dependent function. Because of the vibrational origin,  $d_{ii'}(t_k)$  is periodic, and its time average is null. The period is the same for all  $i$  and  $i'$ .

Using (39), each entry  $r_{ij}$  of  $\mathbf{R}_y$  can be expressed as

$$r_{ij} = \frac{1}{N_s} \sum_k \left[ \sum_{i'} (\bar{a}_{ii'} + d_{ii'}(t_k)) s_{i'}(t_k) + \eta_i(t_k) \right] \left[ \sum_{j'} (\bar{a}_{jj'} + d_{jj'}(t_k)) s_{j'}(t_k) + \eta_j(t_k) \right]^*$$

or

$$r_{ij} = \frac{1}{N_s} \sum_{i'j'k} [(\bar{a}_{i'j'} + d_{i'j'}(t_k))s_{i'}(t_k)] \times [(\bar{a}_{j'j'} + d_{j'j'}(t_k))s_{j'}(t_k)]^* \quad (40a)$$

$$+ \frac{1}{N_s} \sum_{i'k} [(\bar{a}_{i'j'} + d_{i'j'}(t_k))s_{i'}(t_k)]\eta_j(t_k)^* \quad (40b)$$

$$+ \frac{1}{N_s} \sum_{j'k} \eta_i(t_k)[(\bar{a}_{j'j'} + d_{j'j'}(t_k))s_{j'}(t_k)]^* \quad (40c)$$

$$+ \frac{1}{N_s} \sum_k \eta_i(t_k)\eta_j^*(t_k). \quad (40d)$$

Consider a particular element, denoted  $e_{i'j'}$ , of the sum in term (40a) of the previous equation, for a given  $i'$  and  $j'$ :

$$e_{i'j'} = \frac{1}{N_s} \sum_k [(\bar{a}_{i'j'} + d_{i'j'}(t_k))s_{i'}(t_k)][(\bar{a}_{j'j'} + d_{j'j'}(t_k))s_{j'}(t_k)]^*.$$

The entry  $e_{i'j'}$  can be split into

$$e_{i'j'} = \bar{a}_{i'j'} \left[ \frac{1}{N_s} \sum_k s_{i'}(t_k)s_{j'}^*(t_k) \right] \bar{a}_{j'j'}^* \quad (41a)$$

$$+ \frac{1}{N_s} \sum_k d_{i'j'}(t_k)s_{i'}(t_k)s_{j'}^*(t_k)d_{j'j'}^*(t_k) \quad (41b)$$

$$+ \bar{a}_{i'j'} \frac{1}{N_s} \sum_k s_{i'}(t_k)s_{j'}^*(t_k)d_{j'j'}^*(t_k) \quad (41c)$$

$$+ \frac{1}{N_s} \sum_k [d_{i'j'}(t_k)s_{i'}(t_k)s_{j'}^*(t_k)]\bar{a}_{j'j'}^*. \quad (41d)$$

**PROPOSITION** The entries  $t_{ij}(N_s)$  of  $\mathbf{T}(N_s) \rightarrow 0$  when  $N_s \rightarrow \infty$ .

**PROOF** The entries of  $\mathbf{T}(N_s)$  are given by  $t_{ij} = (40b) + (40c) + \sum_{i'j'} [(41c) + (41d)]$ .

We first consider the term (41d) =  $\bar{a}_{j'j'}^*(1/N_s)$

$$\cdot \sum_{k=1}^{N_s} d_{i'j'}(t_k)s_{i'}(t_k)s_{j'}^*(t_k).$$

Assume that a period  $d_{j'j'}(t_k)$  is described by  $n_p$  samples and that there are  $N_p$  periods in the  $N_s$  samples corresponding to the observation time; we have  $N_s = n_p N_p + n_r$  (where  $n_r$ , the remaining number of samples, is always  $< n_p$ ). Obviously, when  $N_s \rightarrow \infty$ , we have  $N_p \rightarrow \infty$  since  $n_p$  is constant and  $n_r < n_p$ .

In (41d), the sum over the samples can then be expressed as

$$(41d) = \frac{\bar{a}_{j'j'}^*}{n_p} \sum_{k=1}^{n_p} d_{i'j'}(t_k) \frac{1}{N_p + (n_r/n_p)} \sum_{l=0}^{N_p-1} s_{i'}(t_{l \times n_p + k}) s_{j'}^*(t_{l \times n_p + k}) + \frac{\bar{a}_{j'j'}^*}{N_s} \sum_{k=1}^{n_r} d_{i'j'}(t_k) s_{i'}(t_k) s_{j'}^*(t_k).$$

For a given  $k$ ,  $s_{i'}(t_{l \times n_p + k})$ , ( $l = 0, \dots, N_p$ ) is a subseries extracted from the  $s_{i'}(t_l)$  ( $l = 1, \dots, N_s$ ) by undersampling. We denote such an undersampled

signal as  $s_{i'}^p(t_l)$ ,  $l = 0, \dots, N_p$ . Assuming that such subseries remain ergodic and stationary, as are their native series, we have

$$\lim_{N_p \rightarrow \infty} \frac{1}{N_p + (n_r/n_p)} \sum_{l=0}^{N_p} s_{i'}(t_{l \times n_p + k}) s_{j'}^*(t_{l \times n_p + k}) = E\{s_{i'}^p s_{j'}^{p*}\} \quad (42)$$

and consequently

$$\lim_{N_p \rightarrow \infty} \frac{\bar{a}_{j'j'}^*}{n_p} \sum_{k=1}^{n_p} d_{i'j'}(t_k) \frac{1}{N_p + (n_r/n_p)} \times \sum_{l=0}^{N_p-1} s_{i'}(t_{l \times n_p + k}) s_{j'}^*(t_{l \times n_p + k}) = \frac{\bar{a}_{j'j'}^*}{n_p} \sum_{k=1}^{n_p} d_{i'j'}(t_k) E\{s_{i'}^p s_{j'}^{p*}\}.$$

Since  $d_{i'j'}(t_k)$  is periodic and its temporal average is null, we can conclude that this limit is equal to zero.

When the magnitudes of signals and vibrations are bounded, there exists an upper bound for the modulus of this previous expression:

$$\left| \frac{1}{N_s} \left| \sum_{k=1}^{n_r} d_{i'j'}(t_k) s_{i'}(t_k) s_{j'}^*(t_k) \right| \right| \leq \frac{n_r}{N_s} \max_{k \in \{1, \dots, n_r\}} |d_{i'j'}(t_k) s_{i'}(t_k) s_{j'}^*(t_k)| < \infty.$$

Since  $n_r < n_p$ , this last upper-bound tends toward 0 when  $N_s \rightarrow \infty$ . Consequently, we have  $\lim_{N_p \rightarrow \infty} (41d) = 0$ . For the same reasons, the term (41c)  $\rightarrow 0$  when  $N_s \rightarrow \infty$ . Taking into account the independence of sources and noise and their centering, similar developments show that (40b) and (40c)  $\rightarrow 0$  when  $N_s \rightarrow \infty$ .

**PROPOSITION** The entries of the matrix

$$(1/N_s) \sum_{k=1}^{N_s} D(t_k) s(t_k) s^H(t_k) D^H(t_k) < \infty \text{ when } N_s \rightarrow \infty.$$

**PROOF** The entries of such a matrix are given by  $\sum_{i'j'} (41b)$ . As in the (41d) expression, the periodic part of (41b) can be isolated to obtain

$$\frac{1}{N_s} \sum_{k=1}^{N_s} d_{i'j'}(t_k) d_{j'j'}^*(t_k) s_{i'}(t_k) s_{j'}^*(t_k) = \left( \frac{1}{n_p} \sum_{k=1}^{n_p} d_{i'j'}(t_k) d_{j'j'}^*(t_k) \times \frac{1}{N_p + (n_r/n_p)} \sum_{l=0}^{N_p-1} s_{i'}(t_{l \times n_p + k}) s_{j'}^*(t_{l \times n_p + k}) \right) + \frac{1}{N_s} \sum_{k=1}^{n_r} d_{i'j'}(t_k) d_{j'j'}^*(t_k) s_{i'}(t_k) s_{j'}^*(t_k). \quad (43)$$

When  $N_s$  tends to  $\infty$ , the last term  $(1/N_s) \sum_{k=1}^{n_r} d_{i'j'}(t_k) d_{j'j'}^*(t_k) s_{i'}(t_k) s_{j'}^*(t_k)$  tends to 0 for the same previous

reasons. Because of the presence of the quadratic expression  $d_{ii'}(t_k)d_{jj'}^*(t_k)$ , the first term in (43) only tends toward a constant when  $N_s$  (then  $N_p$ ) tends to  $\infty$ :

$$\begin{aligned} & \lim_{N_p \rightarrow \infty} \left( \frac{1}{n_p} \sum_{k=1}^{n_p} d_{ii'}(t_k)d_{jj'}^*(t_k) \right. \\ & \quad \times \left. \frac{1}{N_p + (n_r/n_p)} \sum_{l=0}^{N_p-1} s_{i'}(t_{l \times n_p + k})s_{j'}^*(t_{l \times n_p + k}) \right) \\ & = \frac{1}{n_p} \sum_{k=1}^{n_p} d_{ii'}(t_k)d_{jj'}^*(t_k)E\{s_{i'}^p s_{j'}^{p*}\} \end{aligned}$$

and then  $\sum_{i'j'}(1/N_s) \sum_{k=1}^{N_s} d_{ii'}(t_k)d_{jj'}^*(t_k)s_{i'}(t_k)s_{j'}^*(t_k)$  tends toward  $\sum_{i'j'}(1/n_p) \sum_{k=1}^{n_p} d_{ii'}(t_k)d_{jj'}^*(t_k)E\{s_{i'}^p s_{j'}^{p*}\}$  when  $N_s \rightarrow \infty$ .

## ACKNOWLEDGMENT

The authors thank Dr. Bernard Xerri for his suggestions concerning the proof presented in Appendix C.

## REFERENCES

- [1] Friedlander, B., and Weiss, A. J. Effects of modeling errors on the resolution threshold of the MUSIC algorithm. *IEEE Transactions on Signal Processing*, **42**, 6 (June 1996), 1519–1526.
- [2] Ferreol, A., Larzabal, P., and Viberg, M. On the resolution probability of MUSIC in presence of modeling errors. *IEEE Transactions on Signal Processing*, **56**, 5 (May 2008), 1945–1953.
- [3] Dorny, C. N. A self-survey technique for self-cohering of antenna systems. *IEEE Transactions on Antenna and Propagation*, **AP-26**, 6 (Nov. 1978), 877–881.
- [4] Rockah, Y., and Schultheiss, P. M. Array shape calibration using sources in unknown locations, Part 1: Far-field sources. *IEEE Transactions on Acoustics, Speech, and Signal Processing*, **35** (Mar. 1987), 286–299.
- [5] See, C.-M. S., Poh, B.-K., and Cowan, C. F. N. Sensor array calibration using measured steering vectors of uncertain location. In *Proceedings of the IEEE International Conference on Acoustics, Speech, and Signal Processing*, Apr. 21–24, 1997, 3749–3752.
- [6] Porat, B., and Friedlander, B. Accuracy requirements in off-line array calibration. *IEEE Transactions on Aerospace and Electronic Systems*, **33**, 2, Part 1 (Apr. 1997), 545–556.
- [7] Cevher, V., and McClellan, J. H. Sensor array calibration via tracking with the extended Kalman filter. In *Proceedings of the IEEE International Conference on Acoustics, Speech, and Signal Processing*, May 7–11, 2001, 2817–2820.
- [8] Weiss, A. J., and Friedlander, B. Array shape calibration using sources in unknown locations—A maximum likelihood approach. *IEEE Transactions on Acoustics, Speech, and Signal Processing*, **37** (Dec. 1989), 1958–1966.
- [9] Weiss, A. J., and Friedlander, B. Array processing using joint-diagonalization. *Signal Processing*, **50** (1996).
- [10] Flanagan, B. P., and Bell, K. L. Array self-calibration with large sensor position errors. In *Proceedings of the Conference on Signals, Systems, and Computers*, 1999, 258–262.
- [11] Marcos, S. Calibration of a distorted towed array using a propagation operator. *Journal of Acoustical Society of America*, **93**, 4, Part 1 (Apr. 1993), 1987–1994.
- [12] van der Veen, A. J., and Paulraj, A. An analytical constant modulus algorithm. *IEEE Transactions on Signal Processing*, **44** (May 1996), 1136–1155.
- [13] Santori, A., Barrère, J., Chabriel, G., Jauffret, C., and Medynski, D. Array shape self-calibration for large flexible antenna. Presented at the 2007 IEEE Aerospace Conference, Big Sky, MT, Mar. 2007.
- [14] Santori, A., Chabriel, G., Barrère, J., Jauffret, C., and Medynski, D. A modulus compensation algorithm for shape self-calibration of paired sensors based antennas. Presented at the 2007 IEEE Aerospace Conference, Big Sky, MT, Mar. 2007.



**Agnès Santori** received the Engineer Diploma of the Institut des Sciences de l'Ingénieur de Toulon et du Var, France, and a Masters degree in signal and numerical communications from the University of Nice Sophia-Antipolis, France, in 2004.

She is currently pursuing the Ph.D. degree in radar and remote sensing for embedded antenna at the Office National d'Etudes et de Recherches Aéropatiales (ONERA), Salon de Provence, France.



**Jean Barrère** was born in Bayonne, France, in 1961. He received the Ph.D. degree in mechanics from the University of Bordeaux I, France, in January 1990.

From 1990 to 1994, he worked for ELF-Aquitaine (currently Total-Fina-Elf), CERFACS (European Centre for Research and Advanced Training in Scientific Computation), and Aerospatiale (currently EADS), all in Toulouse, France. His work focused on filtration laws in porous media studies and then plane structure design. He is currently a research engineer on the Signal and System Team of IM2NP Laboratory, Université du Sud Toulon-Var, La Garde, France, where his research interests include wave separation in signal processing.



**Gilles Chabriel** was born in Toulon, France, in 1968. In 1992, he received the Microelectronic and Automatic Engineer diploma from the Institut des Sciences de l'Ingénieur de Montpellier (currently Polytech'Montpellier), Montpellier, France, and the Ph.D. degree in engineer sciences from the Université du Sud Toulon-Var (USTV), La Garde, France, in 1997.

Since 1998, he has been an assistant professor in the Sciences and Applied Sciences Department of the USTV, where he teaches electronic and signal processing. On the Signal and System Team of IM2NP Laboratory, USTV, his research is in the area of signal processing, and his interests include real-world source separation.



**Claude Jauffret** was born in France on March 29, 1957. He received the Diplôme d'Etude Approfondies in applied mathematics from the St. Charles University, Marseille, France, in 1981, the Diplôme d'ingénieur from Ecole Nationale Supérieure d'Informatique et de Mathématiques Appliquées de Grenoble, Grenoble, France, in 1983, the title of "Docteur de l'Université" in 1993 and the "Habilitation à Diriger des Recherches" from the Université du Sud Toulon-Var, France.

From November 1983 to November 1988, he worked on passive sonar systems, more precisely on target motion analysis at the GERDSM, France. After a sabbatical year at the University of Connecticut, during which he worked on tracking problems in cluttered environment, he began researching tracking, data fusion, and extraction at the CERDSM, France. Since September 1996, he has been at the Université du Sud Toulon-Var where he teaches statistical signal processing and dynamic linear systems. His current research is in observability and estimation in nonlinear systems as they appear in tracking problems in the Signal and System Team of IM2NP Laboratory.



**Dominique Medynski** graduated from Ecole Nationale Supérieure des Télécommunications, 1975, Paris, France.

He has been involved in antenna and signal processing for radar and underwater acoustics applications. He is presently heading the Electronic Warfare Program at ONERA.